Angiopoietin-like 4 Stimulates STAT3-mediated iNOS Expression and Enhances Angiogenesis to Accelerate Wound Healing in Diabetic Mice

Han Chung Chong[1], Jeremy Soon Kiat Chan[1], Chi Qin Goh[1], Natalia V Gounko[2], Baiwen Luo[3], Xiaoling Wang[1], Selin Foo[1], Marcus Thien Chong Wong[4], Cleo Choong[3], Sander Kersten[5] and Nguan Soon Tan[1,2]

*[1]School of Biological Sciences, Nanyang Technological University, Nanyang Drive, Singapore, Singapore; [2]Institute of Molecular and Cell Biology, Proteos, A*STAR, Singapore, Singapore; [3]School of Materials Science and Engineering, Nanyang Technological University, Nanyang Avenue, Singapore, Singapore; [4]Tan Tock Seng Hospital, Jalan Tan Tock Seng, Singapore; [5]Nutrition, Metabolism and Genomics group, Wageningen Univeristy, Wageningen, The Netherlands.*

Impaired wound healing is a major source of morbidity in diabetic patients. Poor outcome has, in part, been related to increased inflammation, poor angiogenesis, and deficiencies in extracellular matrix components. Despite the enormous impact of these chronic wounds, effective therapies are lacking. Here, we showed that the topical application of recombinant matricellular protein angiopoietin-like 4 (ANGPTL4) accelerated wound reepithelialization in diabetic mice, in part, by improving angiogenesis. ANGPTL4 expression is markedly elevated upon normal wound injury. In contrast, ANGPTL4 expression remains low throughout the healing period in diabetic wounds. Exogenous ANGPTL4 modulated several regulatory networks involved in cell migration, angiogenesis, and inflammation, as evidenced by an altered gene expression signature. ANGPTL4 influenced the expression profile of endothelial-specific CD31 in diabetic wounds, returning its profile to that observed in wild-type wounds. We showed ANGPTL4-induced nitric oxide production through an integrin/JAK/STAT3-mediated upregulation of inducible nitric oxide synthase (iNOS) expression in wound epithelia, thus revealing a hitherto unknown mechanism by which ANGPTL4 regulated angiogenesis via keratinocyte-to-endothelial-cell communication. These data show that the replacement of ANGPTL4 may be an effective adjunctive or new therapeutic avenue for treating poor healing wounds. The present finding also confirms that therapeutic angiogenesis remains an attractive treatment modality for diabetic wound healing.

Received 6 January 2014; accepted 11 May 2014; advance online publication 1 July 2014. doi:10.1038/mt.2014.102

INTRODUCTION

Impaired wound repair is a major complication of diabetes, resulting in substantial morbidity, lost productivity, and healthcare expenditures. Furthermore, a poor healing diabetic wound is an open portal for infections, often resulting in chronic inflammation, sepsis, dehiscence, and death. Despite the enormous impact of these chronic wounds, effective therapies remain lacking. Effective management of these problems will require better understanding of the healing process to allow the creation of a salubrious physical and biochemical environment conducive to healing.[1]

Normal wound healing proceeds via a continuum of events, including phases of acute inflammation, proliferation, and maturation.[2] The diabetic state induces alterations of all three of these physiological processes.[3] Diabetic wounds are characterized by accumulation of devitalized tissue, increased/prolonged inflammation, poor wound-related angiogenesis, and deficiencies in extracellular matrix (ECM) components.[4] Diabetic wounds show elevated levels of matrix metalloproteinases and increased proteolytic degradation of ECM components, culminating in a corrupt microenvironment that cannot support healing.[3,5] Cells such as keratinocytes, fibroblasts, and endothelial cells also display dysregulated expressions of and responses to many growth factors and cytokines. These features typically make diabetic wounds poorly responsive to most treatments, and thus it may be most advantageous to intervene with aggressive strategies that could improve the corrupt extracellular microenvironment. In this respect, the role of matricellular proteins in wound healing is of interest. Matricellular proteins can associate with the diverse proteins of the ECM reservoir, bridging them with cognate cell surface receptors. They reside at the crossroads of cell–matrix communication, modulating several regulatory networks.[6] Presumably, the regulatory pathways consist of complex networks, creating many opportunities for the compensatory adjustments required for wound repair. Hence, it may be more efficacious to target or replace the necessary matricellular proteins than individual cytokine-mediated candidates.

Angiopoietin-like 4 (ANGPTL4) is a recently identified matricellular protein that is implicated in wound healing.[7,8] It undergoes proteolytic cleavage after secretion, releasing the N-terminal coiled-coil domain (nANGPTL4) and a C-terminal

Correspondence: Nguan Soon Tan, School of Biological Sciences, Nanyang Technological University, 60 Nanyang Drive, Singapore 637551. E-mail: nstan@ntu.edu.sg; nstan@imcb.a-star.edu.sg.

fibrinogen-like domain (cANGPTL4). nANGPTL4 modulates the activity of lipoprotein lipase.[9] We previously showed that cANGPTL4 facilitates keratinocyte migration and wound reepithelialization. Wounds in ANGPTL4-knockout mice exhibit delayed healing and share many characteristics of diabetic wounds, including reduced expression of matrix proteins, increased inflammation, and impaired wound-related angiogenesis.[7,8] ANGPTL4 reportedly also has a context-dependent role in angiogenesis and vascular permeability.[10,11] However, the expression and role of ANGPTL4 in diabetic wound healing remains unclear, and the mechanism by which ANGPTL4 regulates wound angiogenesis is unknown. This study investigated the regulation of wound angiogenesis by ANGPTL4 and examined the potential impact of ANGPTL4 on diabetic wound healing.

RESULTS

Reduced ANGPTL4 expression in impaired diabetic wound healing

First, we characterized the spatiotemporal expression profile of ANGPTL4 messenger ribonucleic acid (mRNA) and protein during the healing of full-thickness excisional splint wounds in ob/+ (normal) and ob/ob (diabetic) mice. Macroscopic observation on days 7–10 postinjury revealed that wounds of ob/ob mice were closed by 40%, while those of ob/+ mice were completely closed (**Figure 1a** and **Supplementary Figure S1a**). Hematoxylin and eosin staining of day-3, -5, -7, and -10 postwound sections showed impaired epithelial regeneration and formation of granulation tissue in ob/ob compared with ob/+ mice. Histomorphometric analysis of centrally dissected ob/ob wound sections revealed significantly delayed re-epithelialization between days 3–10 postwounding (**Figure 1b**). On day 10 postinjury, the epidermal wound area above the wound bed in ob/ob mice remained larger than in ob/+ mice (**Supplementary Figure S1b**). Quantitative real-time PCR (qPCR) revealed reduced ANGPTL4 mRNA levels at day 3 postwounding in ob/ob compared with ob/+ mice (**Figure 1c**). Consistently, immunoblot analysis showed approximately five-fold reduction in cANGPTL4 protein level at day 5 postwounding (**Figure 1d**), and immunofluorescence staining of ANGPTL4 revealed lower signals in wound epithelia and wound bed in ob/ob compared with ob/+ wounds (**Supplementary Figure S1c**). Similar observations were also obtained from wounds of alloxan-induced diabetic mice (data not shown). Antibody specificity was determined by infrared western blot and immunostaining analysis using skin biopsies from wild-type (ANGPTL4$^{+/+}$)

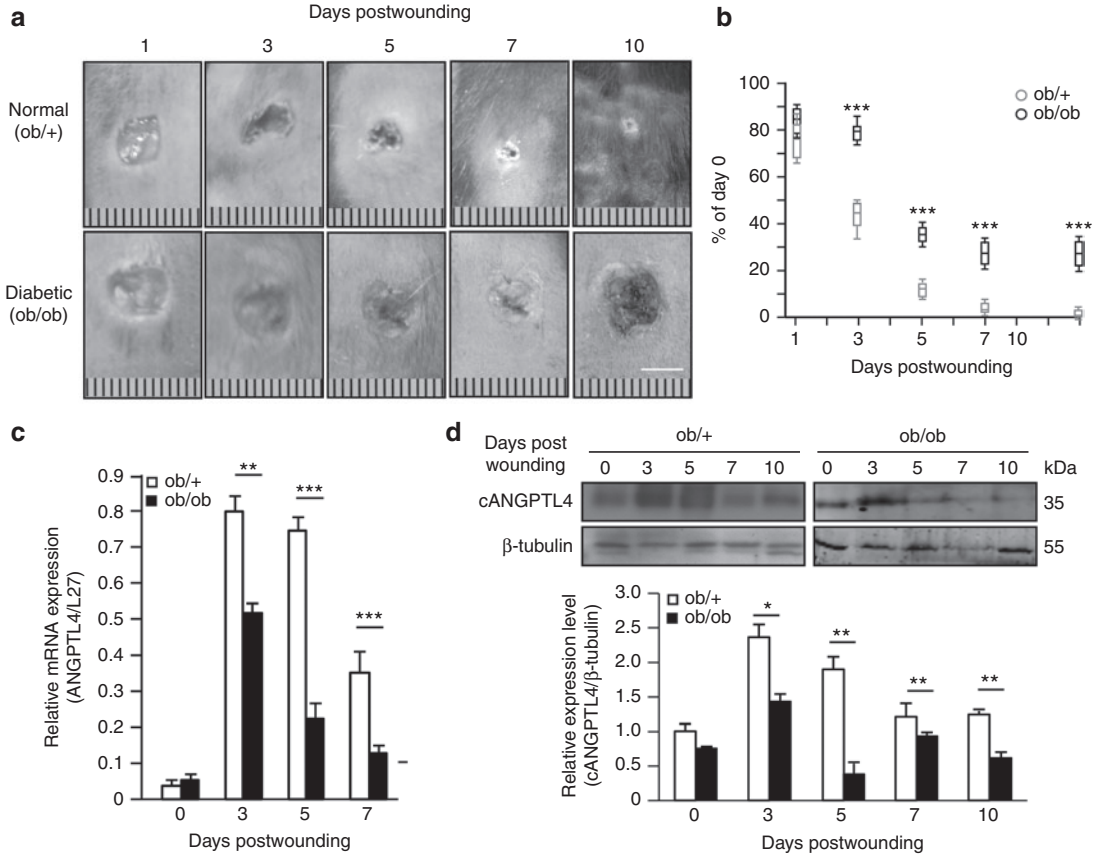

Figure 1 Expression of ANGPTL4 was reduced in diabetic wounds. (**a**) Photos of normal (ob/+) and diabetic (ob/ob) wound biopsies taken at days 1, 3, 5, 7, and 10 postwounding. Bar = 5 mm. (**b**) Wound closure kinetics of ob/+ and ob/ob mice, with wound surface areas plotted as percentage of day 0 (100%). Data are mean ± SEM, $n = 12$. ***$P < 0.001$. (**c**,**d**) Relative ANGPTL4 mRNA (**c**) and protein (**d**) levels in ob/+ and ob/ob wound biopsies as analyzed by qPCR and immunoblotting, respectively. Graph shows the relative cANGPTL4 protein level compared to in the day 0 wound in ob/+ mice. qPCR values were normalized to the housekeeping gene ribosomal protein L27. β-tubulin served as a loading and transfer control for immunoblotting. Data are mean ± SEM, $n = 12$. *$P < 0.05$, **$P < 0.01$, ***$P < 0.001$. ANGPTL4, angiopoietin-like 4; qPCR, quantitative real-time PCR.

and ANGPTL4-knockout (ANGPTL4$^{-/-}$) mice (**Supplementary Figure S2a,b**).

Topical application of cANGPTL4 improves the healing rate of diabetic wounds

Next, we examined the effect of a single topical application of recombinant cANGPTL4 on the diabetic wound healing rate. We inflicted two full-thickness excisional splint wounds on the dorsal skin of ob/ob mice: one to be treated with saline and the other with cANGPTL4 (**Supplementary Figure S3a**). Wound images at days 7 and 10 postinjury showed improved wound closure with cANGPTL4 treatment compared with saline treatment (**Supplementary Figure S3b**). Histomorphological examination of wound sections showed that cANGPTL4 significantly accelerated reepithelialization compared with saline controls, as indicated by the reduced epithelial gap (**Figure 2a**

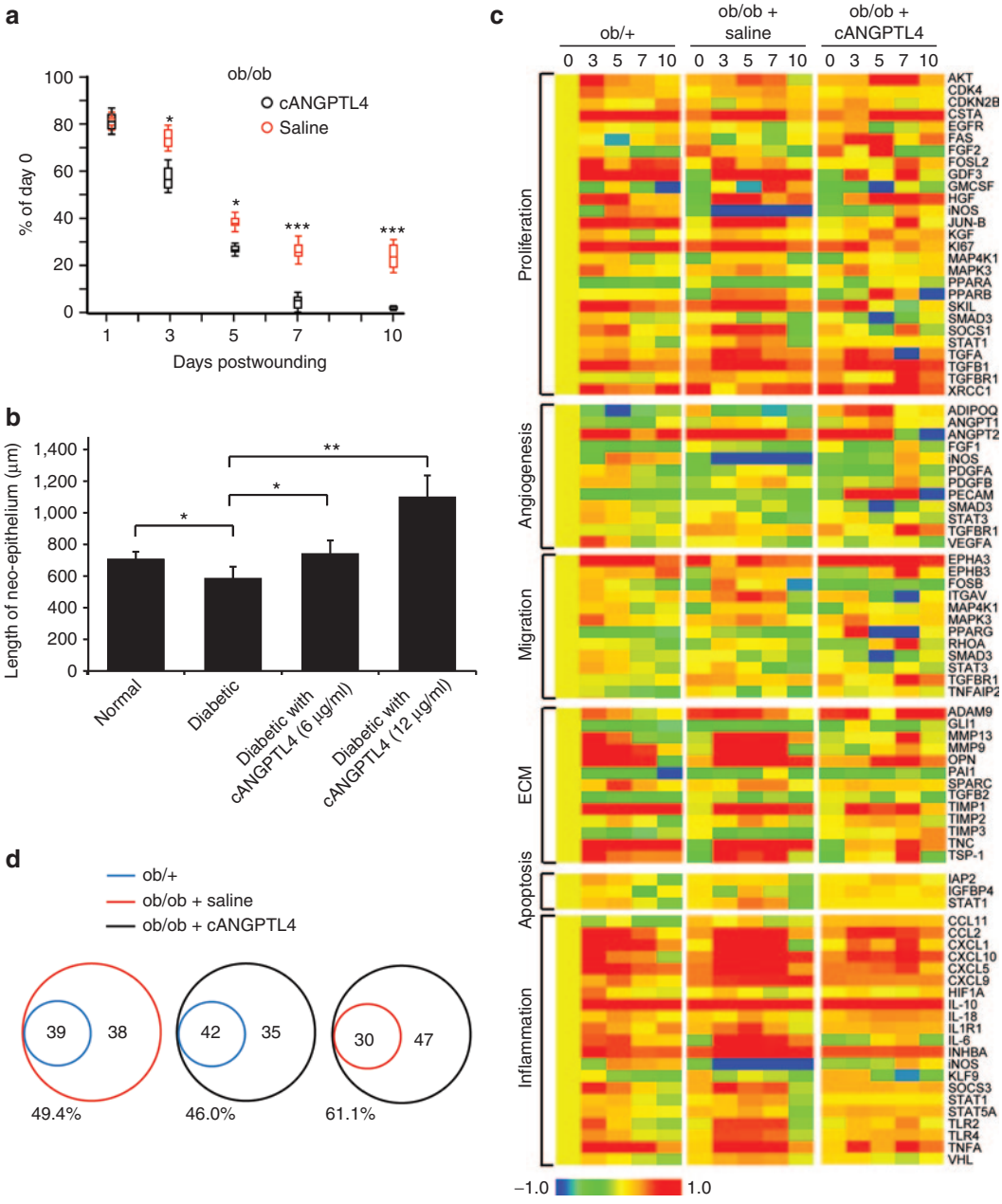

Figure 2 Topical application of ANGPTL4 improves diabetic wound healing. (**a**) Wound closure kinetics of saline- and cANGPTL4-treated ob/ob wounds, with wound surface areas plotted as percentage of day 0 (100%). Data are mean ± SEM, $n = 12$. *$P < 0.05$, **$P < 0.01$. (**b**) Average lengths of neo-epithelium from human skin biopsies cultured for 5 days under normal and diabetic conditions with various cANGPTL4 concentrations. Data are mean ± SEM, $n = 12$. *$P < 0.05$, **$P < 0.01$. (**c**) Heat maps show gene expression profiles of ob/+, and saline- and cANGPTL4-treated ob/ob wounds. Genes are clustered according to the following biological gene functions: proliferation, angiogenesis, migration, ECM, apoptosis, and inflammation. The colour spectrum from blue to red depicts the fold-change in LOG form from –1.0 to 1.0. (**d**) Venn diagram comparing total number of genes from ob/+ (blue), and saline- (red) and cANGPTL4-treated (black) ob/ob wounds. Comparisons of the percentages of total numbers of genes changed. ANGPTL4, angiopoietin-like 4.

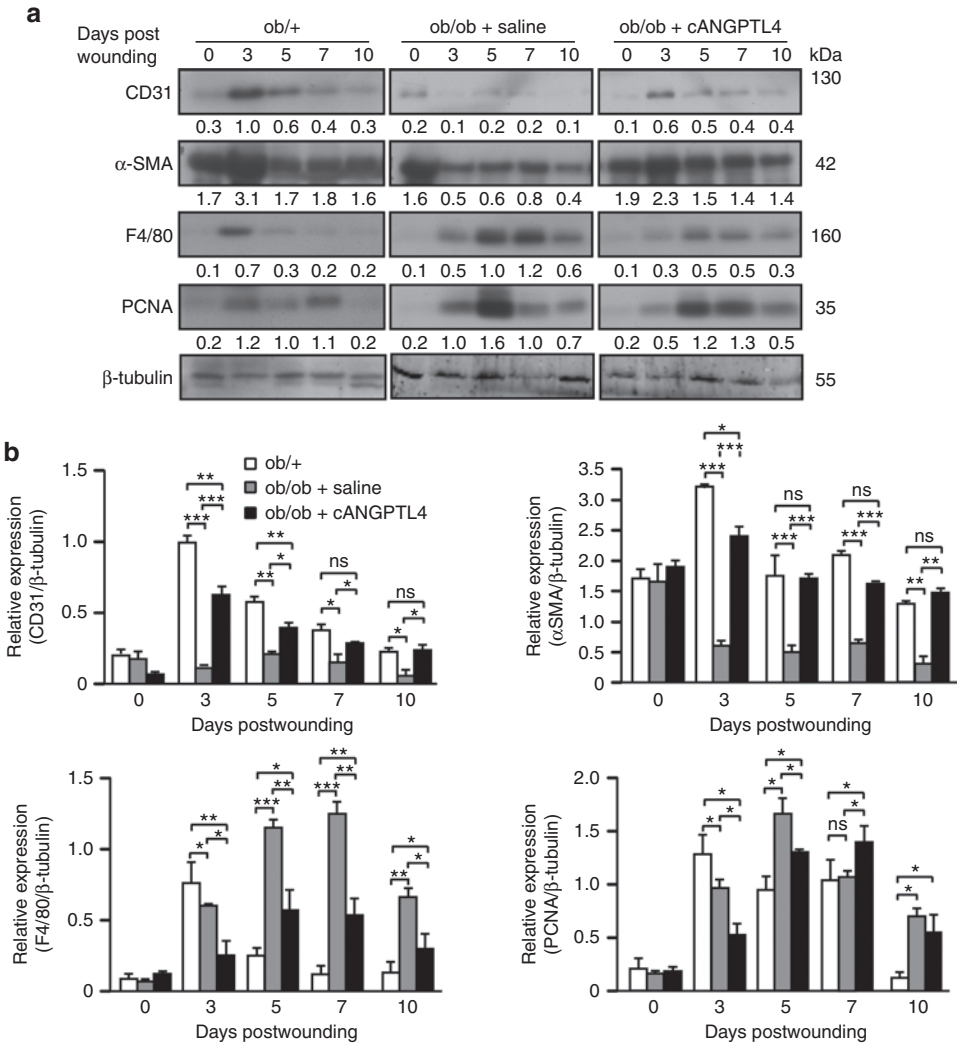

Figure 3 ANGPTL4 improves wound-related angiogenesis. (**a**) Representative immunoblots and (**b**) graph showing relative protein levels of indicated proteins from ob/+, and saline- and cANGPTL4-treated ob/ob wound biopsies. The graph was determined based on the mean densitometry value of the immunoblot obtained from three independent sets of mice wounding experiments. The data was normalized against the densitometry value of β-tubulin, which served as a loading and transfer control. Data are mean ± SEM, $n = 12$ mice per set. *$P < 0.05$; **$P < 0.01$, ***$P < 0.001$ by unpaired Student's *t*-test. ANGPTL4, angiopoietin-like 4.

and **Supplementary Figure S3c**). Similarly, the length of neoepithelia from human skin biopsies was significantly dose-dependently increased in the diabetic-like condition with cANGPTL4 treatment compared to in normal or diabetic conditions without cANGPTL4 (**Figure 2b** and **Supplementary Figure S3d**).

Aberrant growth factor production and activation of cognate signaling cascades contribute to poor diabetic wound healing. To investigate if treatment of diabetic wounds with cANGPTL4 affected their expression profiles, we performed focused qPCR arrays on wound biopsies from control ob/+, and saline- and cANGPTL4-treated ob/ob wounds. We analyzed 77 genes clustered according to the biological functions of proliferation, angiogenesis, cell migration, ECM matrix, cell apoptosis, and inflammation. Heat maps revealed significant expression changes in many genes associated with angiogenesis, ECM remodelling, and inflammation (**Figure 2c**; **Supplementary Tables S2-S4**). cANGPTL4-treated ob/ob wounds exhibited a 61.1% change in overall differential gene profile compared to saline-treated ob/ob wounds, suggesting an altered wound healing signature (**Figure 2d**).

ANGPTL4 induces angiogenesis in diabetic wounds

Next, we examined expressions of markers of specific cell types, including endothelial cell nuclear antigen (CD31), myofibroblasts (α-smooth muscle actin (αSMA)), proliferating cell nuclear antigen (PCNA), and macrophages (F4/80). Saline-treated ob/ob wounds displayed reduced CD31 and αSMA expressions from day 3 postwounding compared with ob/+ wounds. F4/80 and PCNA expressions were elevated until day 10 postwounding in saline-treated ob/ob wounds compared with ob/+ wounds, consistent with prolonged inflammation and delayed resolution of wound reepithelialization (**Figure 3a**,**b**). Although the F4/80 and PCNA expression pattern remained unchanged in cANGPTL4-treated ob/ob wounds, the overall expression levels were significantly reduced compared to in saline-treated ob/ob wounds (**Figure 3b**).

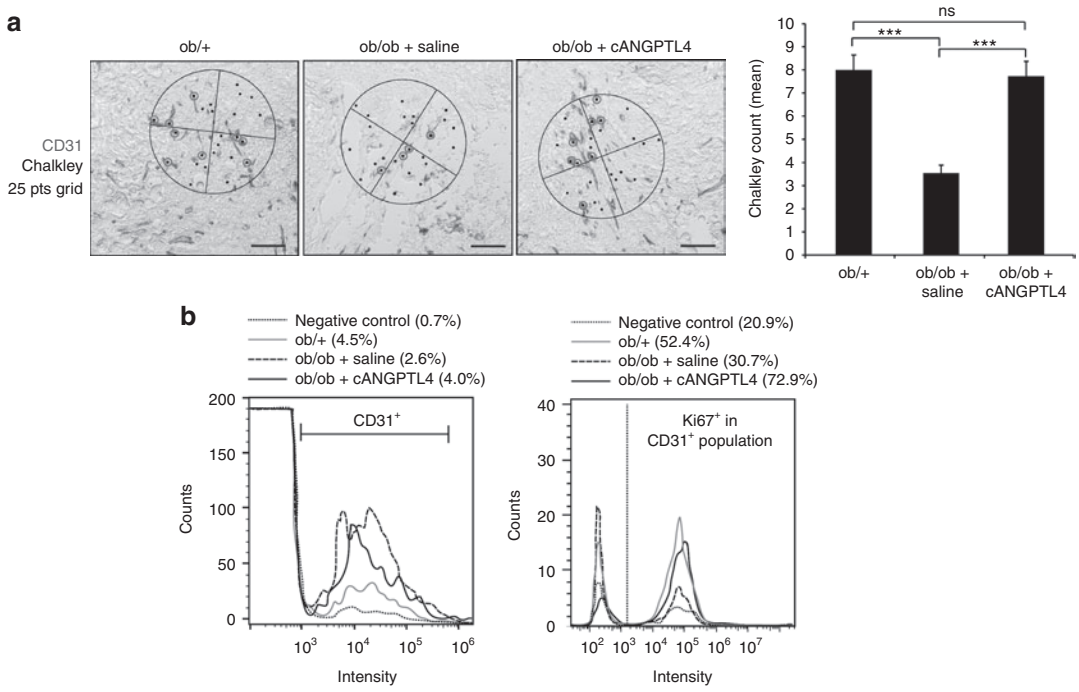

Figure 4 ANGPTL4 induced angiogenesis in ob/ob wound. (**a**) Representative immunostaining for CD31 (brown) on ob/+, and saline- and cANGPTL4-treated ob/ob wound biopsies. Bar = 40 µm. Chalkley's 25 points grids were used to determine the mean chalkley counts shown in the graph for at least three microscopic fields from three independent experiments. Data are mean ± SEM, $n = 9$. ***$P < 0.001$; (**b**) Representative histograms generated from flow cytometry showing percentage of $CD31^+$ endothelial cells population from total cells isolated from ob/+, saline-treated ob/ob and cANGPTL4-treated ob/ob wound biopsies (left panel). Histograms gated from $CD31^+$ endothelial cells population showing percentage of $Ki67^+$ proliferative cells (right panel). ANGPTL4, angiopoietin-like 4.

Notably, the CD31 and αSMA expression profiles in cANGPTL4-treated ob/ob wounds had reverted to those observed in ob/+ wounds (**Figure 3b**). To further strengthen our finding, immunofluorescence staining of Ki67, αSMA and CD31 were performed on day 5 and day7 post-wounding biopsies from ob/+, saline- and cANGPTL4-treated ob/ob mice. No difference was observed in number of Ki67-positive proliferating cells among ob/+, saline- and cANGPTL4-treated ob/ob wounds (**Supplementary Figure S4**). Consistent with the finding from western blots, immunostaining of CD31, and αSMA in cANGPTL4-treated ob/ob wounds have reverted to those observed in ob/+ wounds (**Supplementary Figure S4**).

To determine if ANGPTL4 improves wound angiogenesis, we performed immunofluorescence staining of CD31 and quantitative analysis of CD31-positive isolated cells from various treated day-5 wound biopsies. The Chalkley counting method was applied for analyzing the extent of endothelial tube formation wherein a higher Chalkley count represents better angiogenesis. Chalkley counting method is a morphometric point counting systems using microscope eyepiece graticule and has been recommended as a standard in international consensus reports on the quantification of angiogenesis.[12,13] cANGPTL4 treatment increased CD31 immunohistochemistry staining in ob/ob wounds compared with saline-treated ob/ob wounds (**Figure 4a**, top), indicating increased wound vasculature. The mean Chalkley counts of the cANGPTL4-treated ob/ob wounds was significantly two-fold higher compared to saline-treated ob/ob wounds (**Figure 4a**, bottom). Our fluorescence-activated cell sorting (FACS) analysis showed ~53% increase in $CD31^+$ endothelial cells in cANGPTL4-treated ob/ob wounds compared with saline-treated ob/ob wounds, approaching to the level detected in ob/+ wounds (**Figure 4b**). Furthermore, 72.9% of the $CD31^+$ endothelial cell population in cANGPTL4-treated ob/ob wounds also stained positive for proliferation marker Ki67, compared with only 30.7% and 52.4% ($CD31^+Ki67^+$) for saline-treated ob/ob and ob/+ wounds, respectively. Altogether, these observations indicate that cANGPTL4 improves wound angiogenesis.

To check if ANGPTL4 has any direct effect on the endothelial cells (ECs) survival, we have performed FACS analysis for both apoptosis (annexin and PI staining) and proliferation (incorporation of BrdU) assay on attached ECs in the presence and absence of cANGPTL4. Our results did not show any significant difference on apoptosis and proliferation of cANGPTL4-treated ECs compared with saline-treated ECs (**Supplementary Figure S5**)

ANGPTL4 increases nitric oxide production as an angiogenic mediator in diabetic wounds

Our focused gene array analysis revealed that iNOS expression was dramatically increased in ob/ob wounds treated with cANGPTL4 compared with saline. To understand how ANGPTL4 modulates angiogenesis, we first examined the level of nitric oxide (NO), which is a potent angiogenesis mediator in various time points of our wound biopsies. Using a 4,5-diamino-fluorescein (DAF-FM diacetate) -based assay, we detected an overall NO reduction in ob/ob compared with ob/+ wounds (**Figure 5a**). Furthermore, cANGPTL4-treated ob/ob wounds showed significantly increased

NO production from day 3 postwounding compared to those with saline treatment, suggesting that cANGPTL4 may mediate NO production (Figure 5a).

We further found that, in contrast to ob/+ wounds in which endothelial nitric oxide synthase (eNOS) expression peaked at day 5 postwounding, eNOS expression in ob/ob wounds prematurely and transiently peaked at day 3 postwounding (Figure 5b). cANGPTL4 treatment of ob/ob wounds resulted in an increase in eNOS expression from day 5 postwounding, more closely resembling the expression pattern of ob/+ wounds. The maximal fold-change in eNOS expression was similar between ob/+ and cANGPTL4-treated ob/ob wounds. These observations suggest that the elevation of eNOS in wounds may be a secondary effect. cANGPTL4 also did not modulate eNOS expression in primary human dermal microvascular endothelial cells (Figure 5c). Our results showed that ob/ob wounds expressed little iNOS mRNA compared to

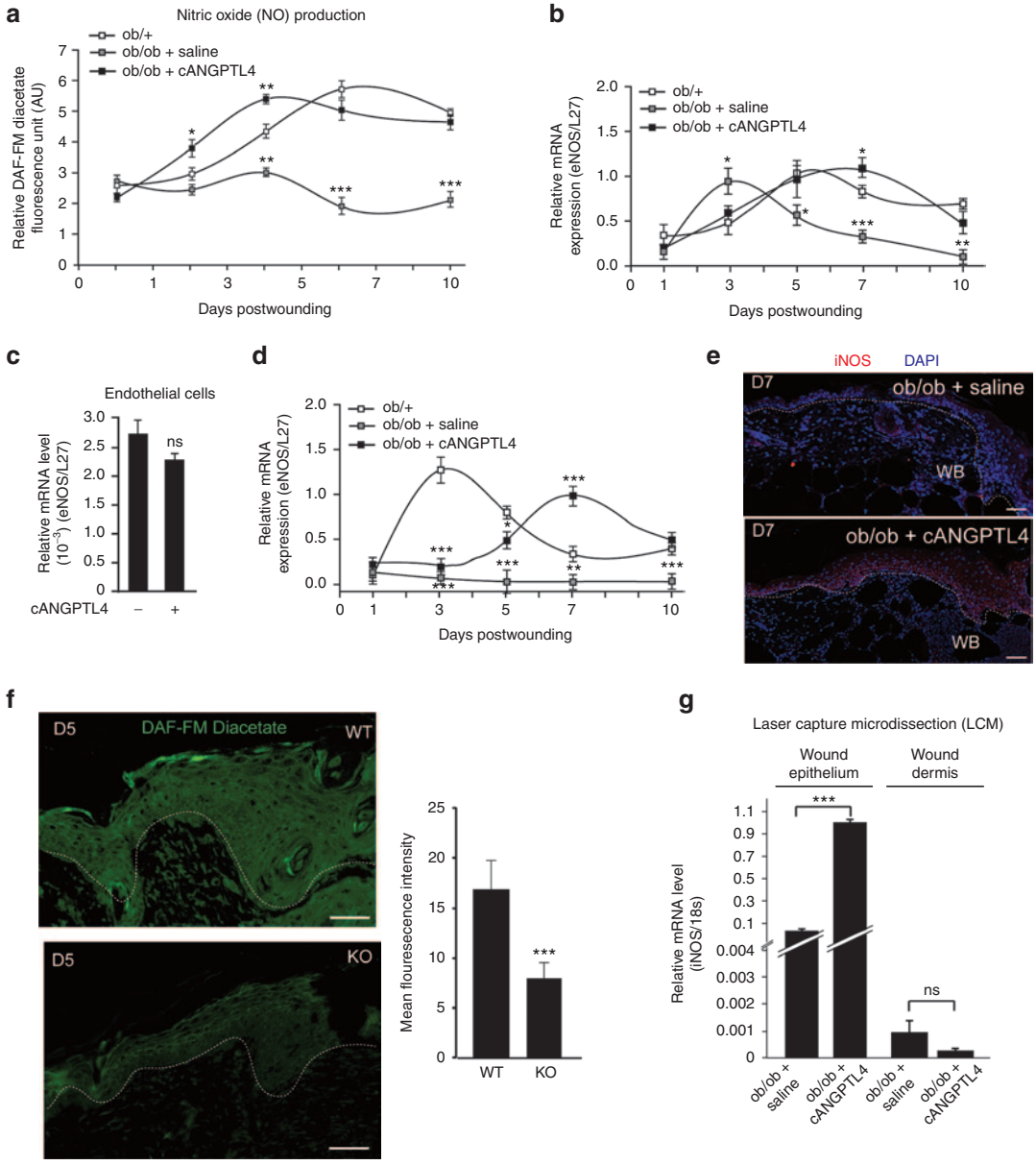

Figure 5 ANGPTL4 regulates NO production in wound epithelium. (**a**) Nitric oxide production in ob/+, and saline- and cANGPTL4-treated ob/ob at indicated postwounding days were determined by measuring the relative DAF-FM diacetate fluorescence level (arbitrary unit, AU). Values were normalized to total protein. (**b**–**d**) Relative mRNA levels of eNOS (**b**) and iNOS (**d**) from indicated wound biopsies, and from primary human dermal microvascular endothelial cells (**c**), as analyzed by qPCR. Values were normalized to the housekeeping gene ribosomal protein L27. (**e**) Immunofluorescence staining of iNOS (red) in day 7 wound biopsies of saline- and cANGPTL4-treated ob/ob mice. Dotted lines delineate the epidermis–dermis interface. Bar = 50 µm. WB, wound bed. (**f**) DAF-FM diacetate fluorescence (green) staining of day 5 post wounding WT and KO mice. Graph shows the mean fluorescence intensity from at least three microscopic fields of three independent mice. Value are mean ± SEM, n = 12. ***P < 0.001 compared to WT mice. (**g**) Expression of iNOS mRNA from laser capture microdissected wound epithelium and wound dermis of saline-treated ob/ob mice and cANGPTL4-treated ob/ob mice. mRNA level were normalized to 18s ribosomal RNA. Data are mean ± SEM, n = 3. ***P < 0.001 compared to saline-treated ob/ob mice. ANGPTL4, angiopoietin-like 4; DAF-FM, 4,5-diamino-fluorescein; KO, knockout; qPCR, quantitative real-time PCR; WT, wild type.

normal ob/+ wounds, in which iNOS expression peaked at day 3 postinjury. cANGPTL4 treatment in ob/ob wounds increased iNOS expression, which peaked at day 7 postinjury (**Figure 5d**). Consistently, our immunofluorescence staining for iNOS showed increased intensity in day-7 cANGPTL4-treated wounds compared with saline controls (**Figure 5e**). To further strengthen our findings, we examined the NO level of ANGPTL4-knockout (KO) mice. Postwounding biopsies from KO mice have significantly lower level of NO detected in the wound epithelium by DAF staining when compared to wild-type (WT) mice (**Figure 5f**). In addition, we separately examined the mRNA expression of iNOS in laser capture microdissected wound epithelia and dermis from the day 7 postwound biopsies of ob/ob mice (**Figure 5g** and **Supplementary Figure S6**). The iNOS mRNA level in the epithelia of cANGPTL4-treated wounds was 10-fold higher than in saline-treated controls. cANGPTL4 treatment of ob/ob wounds did not affect dermal fibroblast iNOS mRNA expression, indicating a cell type-specific response.

To confirm the roles of iNOS and NO induction of angiogenesis and improvement of diabetic wound healing, we cotreated ob/ob wounds with cANGPTL4 and aminoguandine (AG), a selective iNOS inhibitor. As expected, AG delayed ob/ob wound healing even with cANGPTL4 application, phenocopying saline-treated ob/ob wounds (**Figure 6a**). Histomorphometric analysis of saline-treated, cANGPTL4-treated, and cANGPTL4 plus AG-treated ob/ob wound sections revealed that the percentage of wound closure at day 7 postwounding was lower in both

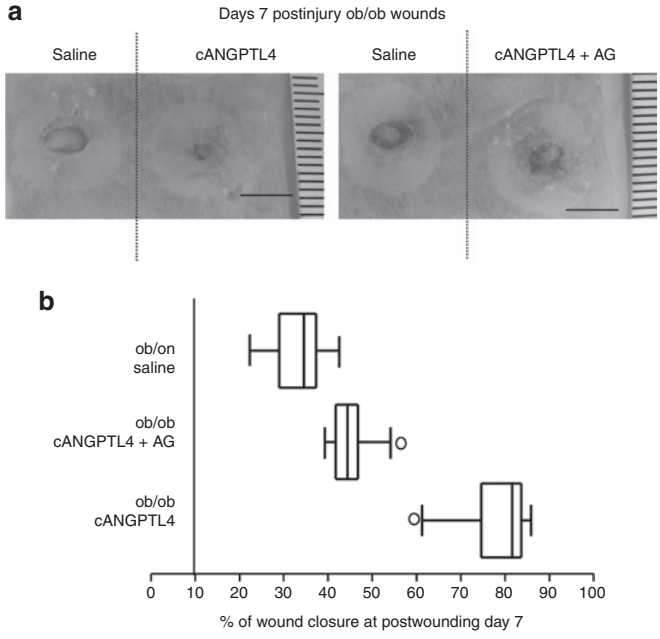

Figure 6 ANGPTL4 regulates iNOS expression. (**a**) Photographs of ob/ob wounds treated with either saline, cANGPTL4 alone, or cANGPTL4 and aminoguanidine (AG). Representative pictures from three independent experiments from are shown. Bar = 5 mm. (**b**) Box and whisker plot of the percentage of wound closure in saline-treated, cANGPTL4-treated, and cANGPTL4 plus AG-treated ob/ob day 7 postwounds biopsies sections. Histomorphometric measurements were determined from 10 independent sections from the various wound biopsies. Middle bar, median; box, interquartile range; whiskers, full value range; *, possible outlier. ANGPTL4, angiopoietin-like 4.

saline-treated and cANGPTL4 plus AG-treated ob/ob wound when compared to cANGPTL4-treated ob/ob wound (**Figure 6b** and **Supplementary Figure S7**). Altogether, these observations suggested that ANGPTL4 stimulates the expression of iNOS in the wound keratinocytes, elevating NO at the wound site to enhance diabetic wound closure rate.

To further strengthen our findings, we have performed *in vitro* tube formation assay using endothelial cells alone or cocultured with keratinocytes in the presence and absence of cANGPTL4. AG, an iNOS inhibitor, was also used in the assay. The tube formation assays were performed under normal and diabetic conditions. Our observation showed that tubule formation was impaired in diabetic conditions, albeit only slightly. Tube formation was not affected by cANGPTL4, regardless of culture conditions. As expected, AG only has little effect. Notably, our result showed that cANGPTL4-accelerated tubule formation only in the presence of keratinocytes which was inhibited by AG (**Supplementary Figure S8**). Thus, the tubule-promoting effect of cANGPTL4 works via a keratinocyte-endothelial cells interaction. (**Supplementary Figure S8**).

ANGPTL4 regulates iNOS expression via STAT3 activation in keratinocytes

To decipher the underlying mechanism of cANGPTL4-mediated acceleration of diabetic wound closure, we first examined the interaction between exogenous cANGPTL4 and integrins in ob/ob wounds using proximity ligation assay (PLA). cANGPTL4 binds to integrin and subsequently activates downstream mediators such as FAK, Src, and ERK to modulate gene expression.[7] PLA signals, visualized as red spots, were increased in cANGPTL4-treated ob/ob wounds compared to saline-treated wounds, suggesting that cANGPTL4 bound and activated integrin β1 (**Figure 7a**, left panel and **Supplementary Figure S9a**). This was confirmed using PLA for active integrin β1 and active Rac1 interactions, which showed increased PLA signals per cell in cANGPTL4-treated compared with saline-treated ob/ob wounds (**Figure 7a**, right panel and **Supplementary Figure S9b**). PLA performed with single specific antibody served as negative controls (**Supplementary Figure S9c**). Immunoprecipitation using anti-cANGPTL4 followed by immunoblot analysis also showed that the activation of downstream mediators such as phosphorylated FAK and Src (**Figure 7b**).

In silico analysis of mouse *iNOS* gene promoter revealed a putative STAT binding site. Immunofluorescence staining showed more phosphorylated STAT3-positive wound keratinocytes in cANGPTL4-treated ob/ob wounds when compared with saline treatment (**Figure 7c**). Keratin 6 identifies hyperproliferative wound keratinocytes. We also examined the JAK/STAT3 activation in day 5 and 7 post-wound biopsies from ANGPTL4 KO and WT mice. Interestingly, the expression of both phosphorylated STAT3 and JAK1 proteins, i.e. activated proteins, was significantly reduced in KO when compared with WT (**Figure 7d**). In addition, immunoblotting of phosphorylated STAT3 and JAK1 proteins from laser microdissected wound epithelia of saline- and cANGPTL4-treated ob/ob wounds clearly showed that cANGPTL4 can activate JAK1/STAT3 signaling in the wound keratinocytes (**Figure 7e**). As expected, this activation of JAK1/STAT3

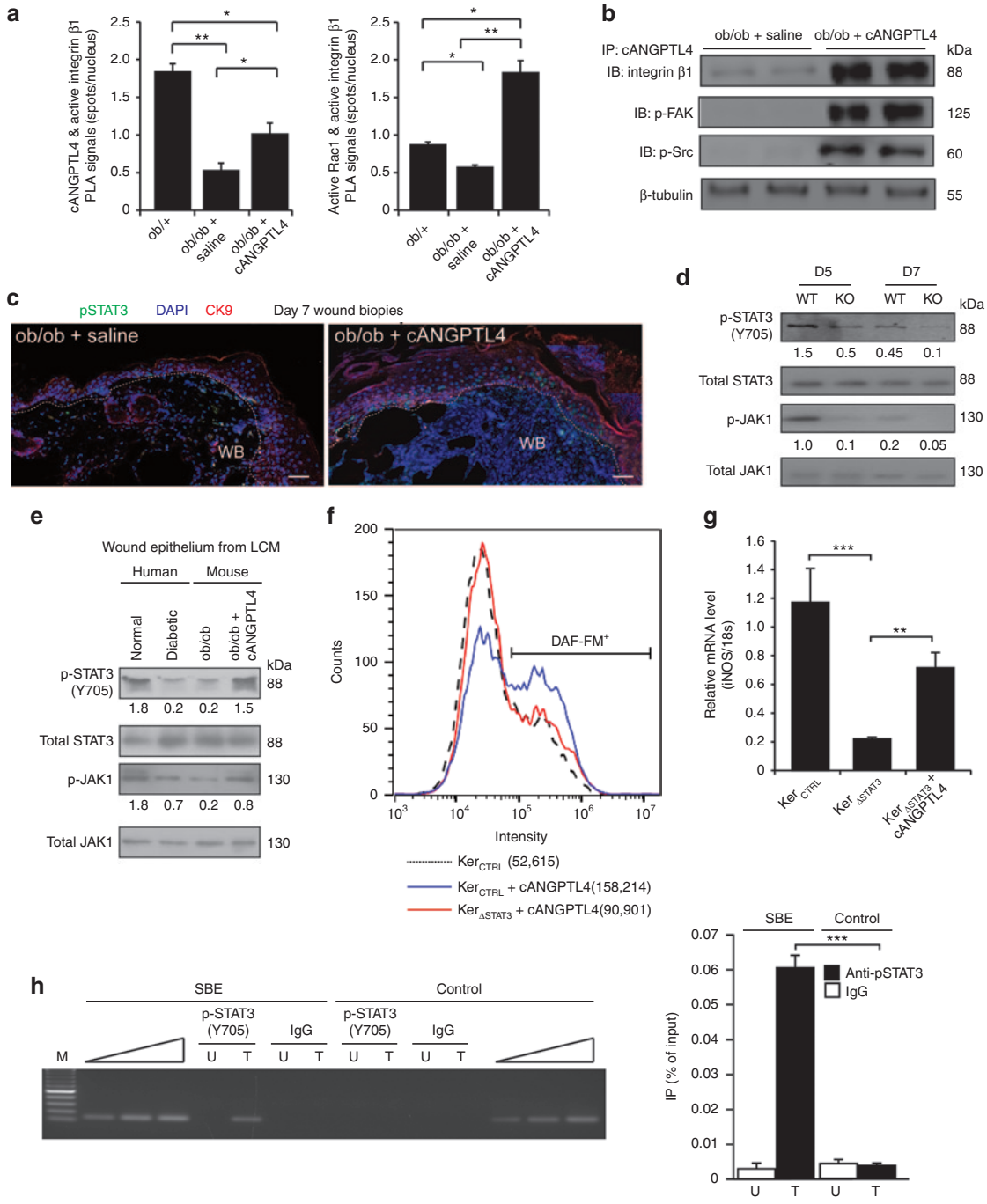

Figure 7 ANGPTL4 activates JAK1/STAT3 signaling to regulate iNOS expression in keratinocytes. (**a**) Quantification of PLA signals of cANGPTL4:active integrin β1 (left panel) and active integrin β1:active Rac1 (right panel). **Supplementary Figure S6** presents representative images of all PLA detections. Each PLA signal indicates one detected interaction event. Number of PLA signals per nucleus was determined using Blobfinder (Uppsala, Sweden) software. Data are mean ± SEM, $n = 3$. *$P < 0.05$, **$P < 0.01$. (**b**) Immunodetection of indicated proteins from anti-cANGPTL4 immunoprecipitates of saline- or cANGPTL4-treated ob/ob wound biopsies. β-tubulin from total tissue lysate was used to verify equal loading. (**c**) Dual immunofluorescence staining of pSTAT3(Y705) (green) and CK6 (red) in saline- and cANGPTL4-treated ob/ob wounds. Dotted lines delineate the epidermis–dermis interface. Nuclei are stained with DAPI (blue). Bar = 40 µm. WB, wound bed. (**d**) Immunodetection of pSTAT3(Y705), total STAT3, p-JAK1, and total JAK1 in postwounding D5 and D7 of both KO and WT mice. (**e**) Immunoblots of pSTAT3(Y705), total STAT3, pJAK1, and total JAK1 from laser capture microdissected epithelium of normal human skin, diabetic human skin, saline-treated ob/ob wound, and cANGPTL4-treated ob/ob wound. (**f**) Representative histograms generated from flow cytometry showing the mean intensity of DAF-FM signal from STAT3 knockdown keratinocytes in the absence or presence of cANGPTL4, Data are mean ± SEM, $n = 3$. (**g**) Relative mRNA expression level of iNOS from STAT3 knockdown keratinocytes in the absence or presence of cANGPTL4, $n = 3$. **$P < 0.01$, ***$P < 0.001$. (**h**) ChIP assays were conducted using preimmune IgG or antibodies against pSTAT3(Y705) in saline- (U) and cANGPTL4-treated (T) ob/ob wounds at day 7 postinjury. Graph (right panel) shows quantitative ChIP as percentage of input. Specific regions spanning promoter binding sites of the *iNOS* gene were amplified using appropriate primers (**Supplementary Table S1**). A control region served as a negative control. ANGPTL4, angiopoietin-like 4; ChIP, chromatin immunoprecipitation; DAF-FM, 4,5-diamino-fluorescein; KO, knockout; PLA, proximity ligation assay; WT, wild type.

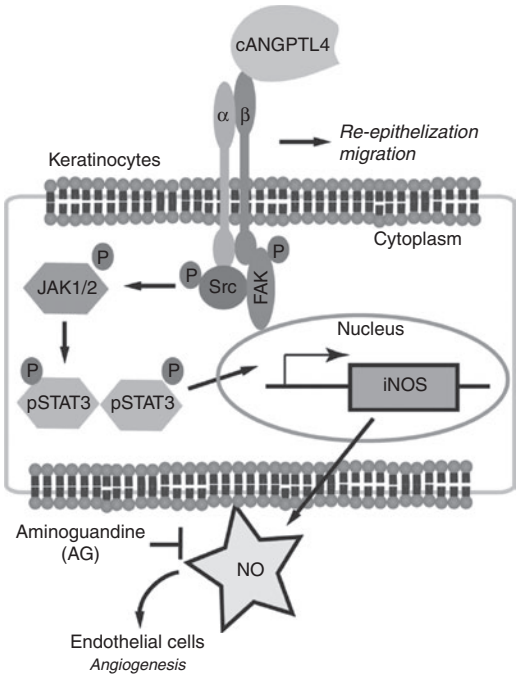

Figure 8 Schematic illustration of the autocrine and paracrine effect of ANGPTL4 on cutaneous wound healing. cANGPTL4 can interact with integrin β1, and activate the Src, ERK, and AKT signaling cascades, leading to subsequent JAK1/STAT3 activation. Activated STAT3 can then mediate the upregulation of iNOS expression by specifically binding to the cognate responsive elements in the promoter of *iNOS* gene. Wound angiogenesis can then be promoted by the increase in NO production from the wound keratinocytes in the wound microenvironment. ANGPTL4, angiopoietin-like 4; PLA, proximity ligation assay.

signaling was also observed in laser microdissected wound epithelium of normal human skin compared to diabetic human skin (**Figure 7e** and **Supplementary Figure S6**). To determine whether cANGPTL4 regulates iNOS expression via STAT3 signaling in keratinocytes, we measured iNOS mRNA by qPCR and NO production using DAF-FM in STAT3-knockdown keratinocytes (Ker_{STAT3}) treated with cANGPTL4. Our result showed reduced iNOS mRNA and NO levels in Ker_{STAT3} compared with Ker_{CTRL} (**Figure 7f,g**).

Finally, *in vivo* chromatin immunoprecipitation showed that phospho-STAT3 specifically bound to the cognate responsive elements in the promoter of the mouse *iNOS* gene in ANGPTL4-treated but not saline-treated ob/ob wounds (**Figure 7h**, left panel). No immunoprecipitation or amplification was seen with preimmune IgG or with a control sequence upstream of the responsive elements in the promoter *iNOS* gene (**Figure 7h**, left panel). Quantitative ChIP showed ~15-fold enrichment in STAT-binding region (SBE) when compared with cognate controls (**Figure 7h**, right panel). Altogether, these observations indicate that ANGPTL4 stimulates NO generation in wound keratinocytes through direct transcriptional regulation of the *iNOS* gene by pSTAT3.

DISCUSSION

Diabetic wounds heal poorly, often resulting in ulceration. Relatively few topical medications are efficacious for ulcer care, and amputation rates remain high in nonhealing diabetic patients. Growing evidence indicates that altered expressions of cytokines and ECM proteins play significant roles in the delayed healing of diabetic wounds. Experimental evidence shows that vascular-endothelial growth factor, platelet-derived growth factor, and epidermal growth factor accelerate diabetic wound healing in animal models[14–16]; however, successful results require high doses of these growth factors. Furthermore, these therapeutic strategies ignore the central coordinating role of the matrix proteins in orchestrating and enhancing the cascade of cellular events in the wound healing response.

Here, we showed that the topical application of recombinant cANGPTL4 accelerated wound reepithelialization in diabetic mice by improving wound angiogenesis. The matricellular protein cANGPTL4 expression has been weakly detected in normal intact skin and is markedly elevated upon wound injury. In contrast, cANGPTL4 expression remains low throughout the healing period in diabetic wounds. Topical application of cANGPTL4 modulates several regulatory networks involved in cell migration, angiogenesis and inflammation, as evidenced by an altered wound healing gene expression signature when compared with saline-treated diabetic wounds.

Various studies have suggested that the role of ANGPTL4 in angiogenesis may be context-dependent. Conflicting roles for ANGPTL4 in tumor vascularization have been reported.[17,18] In a model of oxygen-induced retinopathy, pathological neovascularization was strongly inhibited in ANGPTL4-deficient mice.[19] A recent study showed that ANGPTL4 improves the cerebral vasculature network after brain injury and displays vasculoprotective properties when used as an adjunct to vascular-endothelial growth factor.[20] Evidence from ANGPTL4-knockout mice indicates that ANGPTL4 is proangiogenic in normal wound healing.[7] These observations suggest a role for ANGPTL4 in angiogenesis, although the underlying mechanism remains unresolved. Here, we showed that ANGPTL4 has a dramatic influence in the expression profile of endothelia-specific CD31 in diabetic wounds, returning its profile to that observed in wild-type wounds. cANGPTL4 induces NO production through an integrin/JAK/STAT3-mediated upregulation of iNOS expression in diabetic skin, thus revealing a hitherto unknown mechanism by which ANGPTL4 regulates angiogenesis via keratinocyte-to-endothelial-cell communication (**Figure 8**). Interestingly, impaired wound angiogenesis was also observed in mice that lack α3β1 integrin in epidermis, lending support for a keratinocyte-to-endothelial-cell crosstalk that is dependent on epithelial integrin-mediated signaling.[21] PLA and coimmunoprecipitation analysis revealed that exogenous cANGPTL4 interacted with integrin β1. ANGPTL4-bound integrins activated downstream mediators such as Rac1 and JAK. We further showed that ANGPTL4 regulates iNOS expression via STAT3 activation in keratinocytes as evidenced by immunoblot analysis of microdissected wound epithelia, STAT3-knockdown keratinocytes and *in vivo* chromatin immunoprecipitation. Vascular-endothelial growth factor is a potent angiogenic factor that can also modulate NO generation via eNOS upregulation.[22] In contrast to vascular-endothelial growth factor, cANGPTL4 had little effect on eNOS expression, but clearly induced iNOS expression. We observed that ANGPTL4 treatment shifted

the eNOS expression peak to day 7 postwounding, which is most likely due to the increase in proliferating endothelial cells ($Ki67^+CD31^+$) already detected in the day-5 wounds. Numerous studies have shown that NO can profoundly impact angiogenesis, and we are only beginning to understand the mechanism for its observed beneficial effect on wound repair.[23,24]

Inflammation plays both positive and negative roles in cutaneous repair—the level and length of inflammation can dictate both the healing time and quality of repair.[25] Recapitulating the dampened inflammatory responses found in foetal and adult chronic wounds has proved useful in accelerating repair and reduced scarring.[26,27] We observed that expression of the macrophage marker F4/80 was reduced upon treatment with cANGPTL4 compared to saline, suggesting that cANGPTL4 may reduce wound inflammation. The relationship between ANGPTL4 and inflammation remains unclear. ANGPTL4 has been implicated in other inflammation-associated pathologies; it plays a protective role against the severe proinflammatory effects of saturated fat, as well as in arthritis (particularly in models dependent on adaptive immunity) and in atherosclerosis. The underlying mechanism is unknown and is likely to be highly complex, beyond the scope of this current work.

We have proposed that cANGPTL4 be topically applied to diabetic wounds, which limits systemic circulation and therefore reduces unspecific effects on other tissues and organs. The poorly vascularized state of diabetic wounds further restricts the range of effect of topical cANGPTL4 application. The expression of cANGPTL4 was strongly elevated during normal wound healing, but was absent in the diabetic condition. Hence, our treatment seeks to restore physiological levels of cANGPTL4 functions in diabetic wounds using exogenous recombinant cANGPTL4 proteins. Indeed, the topical application of cANGPTL4 to the wound bed restore expression profile of many crucial wound healing mediators in diabetic wounds closer to that of normal wounds. Our study suggests that the replacement of matricellular protein ANGPTL4 can provide an adjunctive or new therapeutic avenue for treating poor healing wounds such as diabetes-associated ulcers. Furthermore, the present results confirm that therapeutic angiogenesis remains an attractive treatment modality for diabetic wound healing.

MATERIALS AND METHODS

Reagents. We used the following antibodies: Ki67 (NCL-Ki67p) and keratin 6 (NCL-CK6; NovoCastra, Leica Biosystems, Wetzlar, Germany); β-tubulin (H-235, sc-9104), PCNA (PC10, sc-56), αSMA (α-SM1, sc-130617), and goat antirabbit and antimouse IgG-HRP (Santa Cruz Biotechnology, Dallas, TX); CD31 (BD Pharmingen, San Jose, CA); CD68 (FA-11; Biolegend, San Diego, CA); F4/80 (AbD Serotec, Raleigh, NC); STAT3 (ab7966; Abcam, Cambridge, UK); iNOS/NOS II (06-573; Merck Millipore, Billerica, MA); pStat3(Tyr705; #9145; Cell Signaling Technology, Danvers, MA); ID3 (2B11, MA1-23242; Thermo Scientific, Waltham, MA). cANGPTL4 monoclonal antibodies were produced in-house (clone 4A11H5 and 3F4F5). All secondary Alexa Fluor antibodies were from Molecular probes. We used the diaminobenzidine peroxidase substrate kit (Vector Laboratories, Peterborough, UK). Unless mentioned otherwise, all chemicals were from Sigma-Aldrich and molecular biology enzymes from Fermentas. All oligonucleotides were synthesized by Sigma-Proligo (Sigma-Aldrich, Singapore).

Expression and purification of recombinant cANGPTL4. The expression and purification of recombinant cANGPTL4 protein was performed in *Drosophila* S2 cells as described in our previous publication.[8] Recombinant ANGPTL4 proteins were purified from the conditioned medium of stable ANGPTL4-expressing S2 cells by preparative isoelectric membrane electrophoresis.

Animals and wounding experiments. All animal studies were approved and performed in compliance with the regulations of the Institutional Animal Care and Use Committee of Nanyang Technological University. The ANGPTL4-KO mice strain was previously described.[28] Male mice aged 6–8 weeks were used in this study and were individually caged during the wounding experiments. Mice were anesthetized prior to surgery by a single intraperitoneal injection of 80 mg/kg ketamine/10 mg/kg xylazine. Two circular 5-mm full-thickness excisional splint wounds were created, as previously described.[29] On the day of surgery (day 1), 50 µl of recombinant cANGPTL4 protein (1 mg/ml) or PBS in 4% carboxyl methylcellulose (CMC) was topically applied to the wounds and protected with an occlusive dressing (Tegaderm; 3M, Singapore). Mice were euthanized by CO_2 inhalation on days 1, 3, 5, 7, and 10 postwounding. Wound biopsies were subjected to photographic imaging, histomorphometric, and biological analyses. Wound biopsies were processed and wound surface area was determined as previously described.[26,29] Surface wound area at each time-point was expressed as a percentage of initial wound area at day 1 (100%). Histomorphometric measurements of sections were performed as previously described.[7,29]

In vitro *diabetic wound assay.* Human skin tissue samples were provided by Dr. Marcus Wong from Plastic, Reconstructive, and Aesthetic Surgery of Tan Tock Seng Hospital, Singapore under an ethical committee review board approval with reference no. (NHG DSRB Ref: 2012/00071). All human samples had been deidentified subcutaneous adipose was removed. Skin biopsies were made using a 4-mm biopsy punch, and were cultured in DMEM supplemented with 10% foetal bovine serum containing either 5.5 mmol/l glucose and 1 nmol/l insulin (normal condition) or 25 mmol/l glucose and 10 nmol/l insulin (diabetic condition) in a humidified incubator with 5% CO_2 at 37 °C.[30]

Assessment of wound healing. Wounds were photographed at days 1, 3, 5, 7, and 10 postwounding, using a Canon G12 digital camera. Each image included a ruler to allow standard calibration of measurements. Surface wound area was quantified at each time-point, using Image-Pro Plus version 5.1.0.20 software (Media Cybernetics), and was expressed as a percentage of initial wound area at day 1 (100%). Histomorphometric measurements of sections were made through the centre of the wound. Sections of wound biopsies were stained with hematoxylin-eosin. Histological images were visualized with Nikon Eclipse 90i brightfield microscope using a Plan Fluor, 10×/0.30 objective and QCapture Pro version 5.0.1.26 software (QImaging, Canada). The measurements were performed three times from random sections using Adobe Photoshop CS5.1, and the image pixels were calibrated to micrometer using the scale bar.

Laser capture microdissection. Paraffin-embedded sections were mounted onto MembraneSlides 1.0 PEN (Carl Zeiss, Oberkochen, Germany) that was pretreated with UV for 30 minutes. Hematoxylin- and eosin-stained sections were then subjected to laser capture microdissection (LCM) using Arcturus XT laser capture microdissection system according to the manufacturer's instructions (Life Technologies, Carlsbad, CA). LCM tissues were collected onto an adhesive CapSure Macro LCM Caps (Life techonologies).

Immunoblot and western blot analysis for LCM samples. The LCM caps with the captured samples were capped onto 500 µl centrifuging tubes containing 15 µl of lysis buffer and process as previously described.[31] Total RNA was isolated using RecoverAll total nucleic acid isolation (Ambion, Life Technologies) according to the manufacturer protocol. Fifty nanograms of RNA were subjected to Full Spectrum Complete Transcriptome

RNA Amplification (System Biosciences, Mountain View, CA) according to manufacturer's recommendation prior qPCR.

Immunohistochemistry for CD31. Sections were fixed, processed, and blocked as for immunofluorescence staining. Sections were incubated overnight at 4 °C with rat anti-mouse CD31 antibody, followed by incubation with biotinlyated goat anti-rat IgG antibody (Vector laboratories). After incubation with secondary antibodies, sections were incubated in avidin:biotinylated enzyme complex (ABC; Vector Laboratories) for 30 minutes. Sections were developed with 3,3′-diaminobenzidine substrate (Vector Laboratories), which produced a brown stain. Slides were mounted with Fluka Eukitt quick-hardening mounting medium (Sigma-Aldrich). Negative controls did not include the primary antibody. Images were taken using Carl Zeiss MIRAX MIDI using a Plan-Apochromat 20×/0.8 NA objective and Marlin F146.C camera, and MIRAX Viewer Version 1.11.49.0 software (Carl Zeiss Microimaging GmbH, Oberkochen, Germany). Chalkley counting procedure was used for the quantification of capillaries in the wound bed as previously described.[12,13,32,33] Briefly, the three most vascular areas (hot spots) with the highest number of microvessel profiles were chosen subjectively from each wound biopsies. A 25-point Chalkley grid was applied to each area and oriented to permit the maximum number of "hit on" points. The mean Chalkley count was determined.

Chromatin immunoprecipitation. Briefly, biopsies from saline- and cANGPT4-treated ob/ob wounds at day 7 postinjury were cut into small pieces and then digested with 0.5% collagenase I at 37 °C. Cells were retrieved and cross-linked using 0.5% formaldehyde for 10 minutes at 37 °C, followed by sonication in sodium dodecyl sulfate (SDS) lysis buffer (1% SDS, 10 mmol/l ethylenediaminetetraacetic acid, and 50 mmol/l Tris-HCl, pH 8.1) to obtain cross-linked DNA of 200–500 bp in length. Of the supernatant, 10% was used as input, while the remaining amount was used to for complexes with pSTAT3(Y705) specific antibody (Cell Signaling Technology) or preimmune IgG. Complexes were pulled down by Protein A/G (Santa Cruz) and were eluted with elution buffer (1% SDS, 0.1 mol/l $NaHCO_3$). DNA fragments were reverse cross-linked at 65 °C for 6 hours. PCR was performed with 5–10 µl of the eluate, using primers flanking either the STAT-binding site of the iNOS gene (−942 to −934) or an unrelated control sequence (>2 kbp away from the binding site). The primer pairs used are presented in **Supplementary Table S1**.

Immunoblotting. Wound biopsies were homogenized with ice-cold protein lysis buffer (20 mmol/l $Na_2H_2PO_4$, 250 mmol/l NaCl, 1% Triton X-100, 0.1% SDS, and 1 mmol/l phenylmethanesulfonyl fluoride; pH 8.0). Total protein lysates were resolved using 10% SDS-PAGE and electrotransferred onto Immobilon-FL polyvinylidene fluoride membrane (IPFL00010, Merck Millipore). Membranes were blocked with 1× Odyssey Blocking buffer (#927–40000, LI-COR Biotechnology, USA) for 1 hour at room temperature. The membrane was then incubated overnight at 4 °C with the indicated primary antibodies in 0.5× Odyssey Blocking buffer diluted with TBST (50 mmol/l Tris HCl, pH 7.6, 150 mmol/l NaCl, and 0.05% Tween-20). Membranes were washed thrice with tris-buffered saline with Tween 20 (TBST), and incubated with appropriate IRDye680- or 800-conjugated anti-IgG secondary antibodies (1:10,000, LI-COR Biotechnology) for 1 hour at room temperature. Protein bands were revealed using the Odyssey CLx Infrared Imaging System, and signals were quantified using ImageStudio Software (LI-COR Biotechnology). To detect cANGPTL4, the membrane was blocked overnight at 4 °C with 1× Odyssey Blocking buffer. The membrane was then incubated overnight at 4 °C with anti-cANGPTL4 mouse monoclonal antibodies (clone 4A11H5) at 0.6 µg/cm^2 of the membrane in 0.5× Odyssey Blocking buffer diluted with TBST.

RNA extraction and reverse transcription. Total RNA was extracted using TRIzol Reagent followed by the PureLink Micro-to-Midi Total RNA Purification System (Invitrogen) according to the manufacturer's protocol. Total RNA was quantified based on the A260/A280 absorbance using the Nanodrop ND1000 (Thermo scientific). Total RNA was reversed transcribed using iScript Reverse Transcription Supermix for RT-1PCR (#170–8841, Bio-Rad).

Focused real-time PCR array. Real-time PCR arrays were used to analyze the expression of a focused panel of genes. qPCR was performed with the CFX96 real-time PCR detection system (Bio-Rad), using KAPA SYBR qPCR Universal Master Mix (KAPABiosystems, Wilmington, MA). Melt curve analysis was included to ensure that only one PCR product was formed. Primers were designed to generate a PCR amplification product of 100–250 bp. Only primer pairs yielding unique amplification products without primer–dimer formation were subsequently used for real-time PCR assays. Expression was normalized to that of the housekeeping gene ribosomal protein L27, which did not change under any of the studied experimental conditions. The qPCR primer sequences are available in **Supplementary Table S1**.

Hydroxyproline assay. Wound biopsies were frozen in liquid nitrogen, and then thoroughly homogenized in distilled water. Aliquots of samples (50 µl) were hydrolyzed in 2 N NaOH at 120 °C for 2 hours, and then oxidized with chloramine-T reagent (0.0127 g/ml) for 25 minutes at room temperature. The chromophore was then developed with the addition of *p*-dimethylaminobenzaldehyde reagent (0.3 g/ml dissolved in methanol/hydrochloric acid solution, 2:1 v/v). The absorbance of the formed reddish-hue complex was measured at 550 nm using a SpectraMax M2e Multi-Mode Microplate Reader and SoftMax Pro Microplate Data Acquisition & Analysis Software (Molecular Devices). Trans-4-hydroxy-L-proline (0–300 µg/ml) was included as a standard. The value of unknown hydroxyproline was determined from the standard curve. Weight of wound biopsies was used for normalization.

NO determination. Intracellular level of NO from wound biopsies were measured using cell-permeable DAF-FM diacetate (D23844, Molecular probes, Invitrogen). Wound biopsies were lysed in Krebs buffer, and incubated with 10 µmol/l DAF-FM diacetate for 30 minutes at 37 °C in darkness. We immediately recorded the fluorophore signal at 495 nm excitation and 515 nm emission wavelengths using a GloMax 20/20 Luminometer (Promega). Fluorescence was expressed as arbitrary fluorescence units, and was measured with the same instrument settings for all experiments.

Intracellular staining and flow cytometry. For determination of proliferative endothelial cells, intracellular staining for CD31 and Ki67 was carried out on the cells isolated from fresh wound biopsy. Cells were fixed and permeabilized in 300 µl of cytoperm buffer (0.01% paraformaldehyde with 0.1% NP40 in PBS) for 20 minutes on ice and blocked with 10% normal goat serum in PBS for 30 minutes at room temperature. Following that the cells were incubated with staining buffer (3% NGS in PBS) containing the rat anti-CD31 (1:200) and rabbit anti-Ki67 (1:200) for 30 minutes on ice, followed by incubation with FITC conjugated goat antirat IgG and PE conjugated goat antirabbit IgG secondary antibody for another 30 minutes on ice before flow cytometric analysis. For determination of NO, intracellular staining with cell-permeable DAF-FM diacetate (D23844, Molecular probes, Invitrogen) was carried out on the transfected keratinocytes. Cells were incubated with in DMEM alone phenol red free containing 2 mmol/l of DAF-FM diacetate for 30 minutes in a humidified incubator with 5% CO_2 at 37 °C. Cells were then trypsinized and resuspended with DMEM supplemented with 10% fetal bovine serum phenol red free before flow cytometric analysis. Flow cytometry was carried out using BD Accuri C6 flow cytometer (BD Biosciences) and data analysis was performed using Flowjo software version 7.6.5 (Tree Star).

Transient suppression of STAT3 in keratinocytes. Keratinocytes were seeded at 5×10^4 cells in 6-well culture plates and were incubated overnight in a humidified incubator with 5% CO_2 at 37 °C prior to the

transfection assay. The experimental setups include untreated cells, non-targeting scrambled siRNA and ON-TARGETplus SMARTpool STAT3 siRNA (L-003544-00-0005; Thermo scientific). A final concentration of 5 μmol/l of siRNA and 4 μl DharmaFECT transfection reagent with serum free medium was added to each seeded well according to the manufacture protocol. Transfection medium was replaced with fresh media 16 hours after the transfection and analysis were performed within 24–96-hour posttransfection.

In vitro *endothelial tube formation assay.* Keratinocytes was seeded onto the 3.0 μm transwell inserts with a final density of 4×10^5 cells/insert. The 24-well plates were coated with 100 μl of Matrigel (Becton Dickinson, Bedford, MA). Primary human umbilical vein endothelial cells of <5 passages were then plated in duplicate at a concentration of 4×10^4 cells/well in 400 μl of endo-grow (endothelial cell growth media) medium. Tubule formation was monitored by liver imaging.

Statistical analysis. Statistical analyses were performed using two-tailed Mann-Whitney tests or two-way ANOVA using SPSS v.19 software (IBM Corporation). A P value of <0.05 was considered significant.

SUPPLEMENTARY MATERIAL

Figure S1. Histomorphometric analysis of centrally dissected ob/+ and ob/ob wound sections.
Figure S2. Specificity of monoclonal antibodies against mouse ANGPTL4.
Figure S3. cANGPTL4 improves diabetic wound healing.
Figure S4. Immunofluorescence staining of wound biopsies.
Figure S5. ANGPTL4 has no direct effect on endothelial cells survival and proliferation.
Figure S6. Laser capture microdissection (LCM) of skin specimens.
Figure S7. Aminoguanidine inhibits wound healing by cANGPTL4.
Figure S8. Effect of ANGPTL4 on *in vitro* endothelial tubule formation.
Figure S9. ANGPTL4 activates the integrin signaling pathway.
Table S1. List of primer pairs sequences.
Table S2. Gene expression in ob/+ wound.
Table S3. Gene expression in Saline-treated ob/ob wound.
Table S4. Gene expression in cANGPTL4-treated ob/ob wound.

ACKNOWLEDGMENTS

We thank the National Medical Research Council, Singapore (IRG10may017) for supporting this research. B.L. and J.S.K.C. are recipients of the Nanyang Technological University and Nanyang President's Graduate Scholarships, respectively. H.C.C. designed, performed, and analyzed the experiments in this study, with intellectual input from N.S.T. J.S.K.C., X.W., and S.F. performed some animal studies and provided technical help. C.Q.G., N.V.G., and B.L. performed electron microscopy. M.T.C.W. and C.C. contributed patient material for analysis and provided intellectual input. N.S.T. provided overall coordination with respect to the conception, design, and supervision of the study. H.C.C., J.S.K.C., and N.S.T., wrote the manuscript with comments from co-authors. The authors declare no conflicts of interest for this study.

REFERENCES

1. Coulombe, PA (2003). Wound epithelialization: accelerating the pace of discovery. *J Invest Dermatol* **121**: 219–230.
2. Werner, S and Grose, R (2003). Regulation of wound healing by growth factors and cytokines. *Physiol Rev* **83**: 835–870.
3. Falanga, V (2005). Wound healing and its impairment in the diabetic foot. *Lancet* **366**: 1736–1743.
4. Blakytny, R and Jude, EB (2009). Altered molecular mechanisms of diabetic foot ulcers. *Int J Low Extrem Wounds* **8**: 95–104.
5. Galkowska, H, Wojewodzka, U and Olszewski, WL (2006). Chemokines, cytokines, and growth factors in keratinocytes and dermal endothelial cells in the margin of chronic diabetic foot ulcers. *Wound Repair Regen* **14**: 558–565.
6. Bornstein, P and Sage, EH (2002). Matricellular proteins: extracellular modulators of cell function. *Curr Opin Cell Biol* **14**: 608–616.
7. Goh, YY, Pal, M, Chong, HC, Zhu, P, Tan, MJ, Punugu, L *et al.* (2010). Angiopoietin-like 4 interacts with integrins beta1 and beta5 to modulate keratinocyte migration. *Am J Pathol* **177**: 2791–2803.
8. Goh, YY, Pal, M, Chong, HC, Zhu, P, Tan, MJ, Punugu, L *et al.* (2010). Angiopoietin-like 4 interacts with matrix proteins to modulate wound healing. *J Biol Chem* **285**: 32999–33009.
9. Zhu, P, Goh, YY, Chin, HF, Kersten, S and Tan, NS (2012). Angiopoietin-like 4: a decade of research. *Biosci Rep* **32**: 211–219.
10. Huang, RL, Teo, Z, Chong, HC, Zhu, P, Tan, MJ, Tan, CK *et al.* (2011). ANGPTL4 modulates vascular junction integrity by integrin signaling and disruption of intercellular VE-cadherin and claudin-5 clusters. *Blood* **118**: 3990–4002.
11. Padua, D, Zhang, XH, Wang, Q, Nadal, C, Gerald, WL, Gomis, RR *et al.* (2008). TGFbeta primes breast tumors for lung metastasis seeding through angiopoietin-like 4. *Cell* **133**: 66–77.
12. Vermeulen, PB, Gasparini, G, Fox, SB, Toi, M, Martin, L, McCulloch, P *et al.* (1996). Quantification of angiogenesis in solid human tumours: an international consensus on the methodology and criteria of evaluation. *Eur J Cancer* **32A**: 2474–2484.
13. Vermeulen, PB, Gasparini, G, Fox, SB, Colpaert, C, Marson, LP, Gion, M *et al.* (2002). Second international consensus on the methodology and criteria of evaluation of angiogenesis quantification in solid human tumours. *Eur J Cancer* **38**: 1564–1579.
14. Galiano, RD, Tepper, OM, Pelo, CR, Bhatt, KA, Callaghan, M, Bastidas, N *et al.* (2004). Topical vascular endothelial growth factor accelerates diabetic wound healing through increased angiogenesis and by mobilizing and recruiting bone marrow-derived cells. *Am J Pathol* **164**: 1935–1947.
15. Cheng, B, Liu, HW, Fu, XB, Sun, TZ and Sheng, ZY (2007). Recombinant human platelet-derived growth factor enhanced dermal wound healing by a pathway involving ERK and c-fos in diabetic rats. *J Dermatol Sci* **45**: 193–201.
16. Ko, J, Jun, H, Chung, H, Yoon, C, Kim, T, Kwon, M *et al.* (2011). Comparison of EGF with VEGF non-viral gene therapy for cutaneous wound healing of streptozotocin diabetic mice. *Diabetes Metab J* **35**: 226–235.
17. Ito, Y, Oike, Y, Yasunaga, K, Hamada, K, Miyata, K, Matsumoto, S *et al.* (2003). Inhibition of angiogenesis and vascular leakiness by angiopoietin-related protein 4. *Cancer Res* **63**: 6651–6657.
18. Tan, MJ, Teo, Z, Sng, MK, Zhu, P and Tan, NS (2012). Emerging roles of angiopoietin-like 4 in human cancer. *Mol Cancer Res* **10**: 677–688.
19. Perdiguero, EG, Galaup, A, Durand, M, Teillon, J, Philippe, J, Valenzuela, DM *et al.* (2011). Alteration of developmental and pathological retinal angiogenesis in angptl4-deficient mice. *J Biol Chem* **286**: 36841–36851.
20. Bouleti, C, Mathivet, T, Coqueran, B, Serfaty, JM, Lesage, M, Berland, E *et al.* (2013). Protective effects of angiopoietin-like 4 on cerebrovascular and functional damages in ischaemic stroke. *Eur Heart J* **34**: 3657–3668.
21. Mitchell, K, Szekeres, C, Milano, V, Svenson, KB, Nilsen-Hamilton, M, Kreidberg, JA *et al.* (2009). Alpha3beta1 integrin in epidermis promotes wound angiogenesis and keratinocyte-to-endothelial-cell crosstalk through the induction of MRP3. *J Cell Sci* **122**(Pt 11): 1778–1787.
22. Cudmore, M, Ahmad, S, Al-Ani, B, Hewett, P, Ahmed, S and Ahmed, A (2006). VEGF-E activates endothelial nitric oxide synthase to induce angiogenesis via cGMP and PKG-independent pathways. *Biochem Biophys Res Commun* **345**: 1275–1282.
23. Witte, MB, Thornton, FJ, Tantry, U and Barbul, A (2002). L-Arginine supplementation enhances diabetic wound healing: involvement of the nitric oxide synthase and arginase pathways. *Metabolism* **51**: 1269–1273.
24. Witte, MB and Barbul, A (2002). Role of nitric oxide in wound repair. *Am J Surg* **183**: 406–412.
25. Eming, SA, Krieg, T and Davidson, JM (2007). Inflammation in wound repair: molecular and cellular mechanisms. *J Invest Dermatol* **127**: 514–525.
26. Tan, NS, Michalik, L, Desvergne, B and Wahli, W (2005). Genetic- or transforming growth factor-beta 1-induced changes in epidermal peroxisome proliferator-activated receptor beta/delta expression dictate wound repair kinetics. *J Biol Chem* **280**: 18163–18170.
27. Lanning, DA, Nwomeh, BC, Montante, SJ, Yager, DR, Diegelmann, RF and Haynes, JH (1999). TGF-beta1 alters the healing of cutaneous fetal excisional wounds. *J Pediatr Surg* **34**: 695–700.
28. Desai, U, Lee, EC, Chung, K, Gao, C, Gay, J, Key, B *et al.* (2007). Lipid-lowering effects of anti-angiopoietin-like 4 antibody recapitulate the lipid phenotype found in angiopoietin-like 4 knockout mice. *Proc Natl Acad Sci U S A* **104**: 11766–11771.
29. Tan, NS and Wahli W (2013). Studying wound repair in the mouse. *Curr Protocols Mouse Biol* **3**: 171–185.
30. Lan, CC, Liu, IH, Fang, AH, Wen, CH and Wu, CS (2008). Hyperglycaemic conditions decrease cultured keratinocyte mobility: implications for impaired wound healing in patients with diabetes. *Br J Dermatol* **159**: 1103–1115.
31. Koob, AO, Bruns, L, Prassler, C, Masliah, E, Klopstock, T and Bender, A (2012). Protein analysis through Western blot of cells excised individually from human brain and muscle tissue. *Anal Biochem* **425**: 120–124.
32. Karow, M (2013). Mountaineering pericytes–a universal key to tissue repair? *Bioessays* **35**: 771–774.
33. Armulik, A, Abramsson, A and Betsholtz, C (2005). Endothelial/pericyte interactions. *Circ Res* **97**: 512–523.